Controlled wettability of biphilic patterned surfaces for enhanced atmospheric water harvesting

Joyce Estephan, Marie Panabière, Camille Petit-Etienne, Sebastien Labau, Léo Bon, Jean-Hervé Tortai, Cécile Gourgon

MNE 23 (2024) 100255

Contents lists available at ScienceDirect

Micro and Nano Engineering

journal homepage: www.sciencedirect.com/journal/micro-and-nano-engineering

Controlled wettability of biphilic patterned surfaces for enhanced atmospheric water harvesting

Joyce Estephan *, Marie Panabière, Camille Petit-Etienne, Sebastien Labau, Léo Bon, Jean-Hervé Tortai, Cécile Gourgon

Univ. Grenoble Alpes, CNRS, CEA/LETI-Minatec, Grenoble INP, Institute of Engineering and Management Univ. Grenoble Alpes, LTM, F-38054 Grenoble, France

ARTICLE INFO

Keywords:
Fog harvesting
Dew condensation
Wettability
Plasma treatment
Maskless lithography

ABSTRACT

Water is a vital component for all living organisms, yet persistent water scarcity remains a global challenge. One potential solution lies in replicating the atmospheric water collection mechanism observed in the Stenocara beetle, characterized by a dorsal surface featuring alternating hydrophilic and hydrophobic regions. In this study, we have designed and examined two distinct biphilic patterned surface configurations, integrating various technologies, to mimic the beetle's water collection strategy. Our investigation evaluates the efficiency of these surfaces in both capturing water from fog and condensing water from dew. For fog collection two parameters were the most impactful: the roughness and the wettability contrast between hydrophilic and hydrophobic zones. In contrast, dew condensation was influenced by additional parameters notably the patterns' size and density that directly affect the water contact angle. It is worth noting, however, that the optimal surface for fog collection may not necessarily coincide with the most effective surface for dew condensation. Furthermore, our research includes a comparative analysis between the theoretically predicted volume of water droplet departure and the empirically observed results.

1. Introduction

In recent years, the water scarcity crisis has reached alarming proportions: almost two thirds of the world's population (four billion people) experience severe water scarcity for at least one month a year and half of the world's population could reside in areas facing water scarcity by as early as 2025 [1]. In response to this issue, numerous strategies have been proposed such as water desalination and filtration systems. However, these methodologies are not only expensive but also energy-consuming [2].

Collecting water from the air, through fog harvesting or dew condensing, is a sustainable, low-cost potential solution. Fog forms when tiny water droplets in the air accumulate, usually ranging from 1 to 50 μm in size [3], while dew is the condensed water from the atmosphere that can be collected when the surface temperature drops below the dew point of the atmosphere [4]. Practically, a range of atmospheric water harvesting techniques already exist. Notably, active and passive dewing techniques are developed and various companies are actively engaged in the production of large-scale dewing systems. As for fog harvesting, meshes are strategically placed perpendicular to the direction of the wind to capture fog droplets [5,6]. Nevertheless, these technologies can be optimized through an exploration of various parameters involved in mesh synthesis, the design of fog harvesting surfaces, and the ongoing development of dewing systems.

Drawing inspiration from natural processes, several techniques for collecting atmospheric water have been explored. Among these, the mechanism observed in the Stenocara beetle has garnered significant attention. These beetles possess a unique back surface featuring hydrophilic non-waxy bumps on a waxy hydrophobic surface [7–9]. The principle behind the hydrophobic/hydrophilic interplay is shown schematically on figure S1 in the Supplementary Information. Droplets appear on both hydrophobic and hydrophilic zones, but they are linked to the density of nucleation sites in the case of condensation, and to the impact of microdroplets of liquid water in the case of fog. Furthermore, droplets nucleated or captured on hydrophobic zones easily migrate towards hydrophilic zones, where they coalesce until reaching a critical size which, under the effect of gravity, causes them to fall, enabling them to be collected. In the case of fog, the main difference is that the amount of water present in the atmosphere is 100 times greater [4]. The same patterns are not the most optimized for both types of collection, since a

* Corresponding author.
E-mail address: joyce.estephan@cea.fr (J. Estephan).

https://doi.org/10.1016/j.mne.2024.100255
Received 16 November 2023; Received in revised form 13 March 2024; Accepted 26 April 2024
Available online 30 April 2024

surface on which the droplets are highly mobile is preferable in the case of fog, corresponding to a more hydrophobic surface overall, whereas condensation requires an increase in the density of possible nucleation sites, with nucleation favored on hydrophilic zones. This has been demonstrated by Nioras et al. [10] in the case of motifs with dimensions equal to or greater than 400 µm. In this work, we will also consider the two collection modes (dew and fog).

Efforts to understand the physics of fog and dew collection have improved efficiency, offering diverse perspectives: chemists and material scientists study surface chemistry, mechanical engineers focus on heat transfer and fluid dynamics, and earth scientists analyze natural condensation and collection phenomena [11]. Within surface chemistry researchers, some have focused their efforts on patterning surfaces with distinct wettability contrasts by combining superhydrophobic and hydrophilic zones employing techniques such as electrospraying [12,13], laser direct writing [14,15] and inkjet printing [16]. Various patterns have been explored including straight stripes [16] or interdigitated lines [17], triangles [18] , grooves [19], squares [20] and dots [21].

On the other hand, others have chosen to emphasize the development of hierarchical structures with more subtle variations in wettability [7,22–25] for collecting water from fog or condensing water from dew. These research papers present data on water collection rates. However, comparing these rates proves challenging due to the dependency on test conditions and the fundamental differences in the mechanisms for collecting water from fog and condensing water from dew. All these studies have resulted in several review articles [3,9,26].

Additionally, in the literature, some researchers investigate dew condensation from a heat transfer perspective, aiming to improve the heat transfer coefficient [27–30].

In many publications, the authors study the rates of condensation or fog harvesting on a type of surface for which they vary a single parameter: pattern shape, or roughness. In the case of patterns, the dimensions are generally of the order of several hundred micrometers, or even millimeters, or in a smaller range when the biphilic behavior is based on composite materials including specific particles. It is important to be able to study the impact of these dimensions in a wider range, from the micron to the millimeter. In this work, we have chosen to produce surfaces featuring hydrophobic and hydrophilic zones with variable materials and roughness, in order to analyze all the parameters as a whole.

2. Experimental

To achieve a diverse range of surfaces with various materials and shapes combining hydrophilic and hydrophobic zones, several technological processes were optimized on 4-inch Si wafers. These optimized procedures are outlined in Figure 1 and are based on combinations of optical Ultraviolet lithography, plasma treatment and metal deposition. In our research, we used negative optical resists, specifically OrmoComp from MicroResist Technology (Berlin, Germany), and SU-8 2010.

The procedure of the first method is the following (Schema available in Supplementary Information, figure S2): after spin-coating the desired polymer, we employed a lithography technique using SmartPrint UV equipment from Microlight 3D, that is a maskless lithography tool. By selectively exposing the polymer surface to ultraviolet (UV) light, various patterns could be formed after development. We achieved hydrophobic polymer triangles in relief or hollow hydrophilic silicon triangles with base lengths ranging from 10 µm to 100 µm and pattern densities ranging from 8% to 37%. To enhance the surface characteristics, we subjected it to plasma treatment. For the OrmoComp polymer, a plasma of Cl_2O_2 was employed, while for SU-8, a plasma of O_2 was used. These specific gases were chosen because they played a crucial role in creating the desired nanoscale roughness for their respective materials. Continuing with the surface treatment, we subsequently exposed the surfaces to CF_4 plasma, resulting in the formation of a thin fluorinated layer on the polymer's surface. This layer made the polymer's surface hydrophobic forming CF and CF_2 bonds, but did not react with the silicon surface, which remained hydrophilic. This was confirmed by XPS analysis as detailed in the Supplementary Information (Figure S3). This analysis revealed a distinct fluorine peak at a binding energy of 685 eV within the OrmoComp spectrum, while no such peak was observed in the plasma-treated silicon. Furthermore, comparison of the carbon spectra between untreated OrmoComp and treated silicon highlighted the emergence of CF and CF_2 bonds. The SU-8 spectrum resembled that of OrmoComp, affirming the presence of fluorine. As a result, we successfully generated patterned surfaces featuring a hydrophobic polymer and hydrophilic silicon zones (Figure 1-a).

In the second approach (Schema available in Supplementary Information, figure S4), we initiated the process by subjecting the spin coated polymer surfaces to a plasma treatment using the same gases mentioned previously for OrmoComp and SU-8. A Polyethylene Terephthalate (PET) flexible foil was also roughened with O_2 and CF_4 plasma treatments becoming superhydrophobic (water contact angle (WCA) of 150° and contact angle hysteresis (CAH) lower than 10°). Following this treatment, a 100 nm layer of aluminum was deposited onto the treated surfaces through the use of different masks. Stainless meshes were used to obtain square apertures with sides measuring 210 µm. Triangular apertures with a base measuring 300 µm were also obtained by laser exposure in an aluminum foil. As a result, using these two masks, we successfully generated metallic hydrophilic patterns on a hydrophobic polymer surface (see Figure 1-b). Atomic Force Microscopy (AFM analysis) revealed that OrmoComp surfaces treated with Cl_2O_2 and CF_4 exhibit minimal roughness, with a root mean square roughness (R_q) of just 15 nm (Figure S5-a). In contrast, SU-8 surfaces subjected to O_2 and CF_4 treatment can exhibit either moderate roughness, with an R_q of 78 nm (Figure S5-b), or a significantly higher roughness, measuring 164 nm (Figure S5-c), depending on whether thermal paste was used to fix the sample during plasma processing or not. The roughened PET displays low roughness with $R_q = 41$ nm.

In addition, we prepared homogeneous samples with hydrophilic and hydrophobic properties, serving as reference points. For the hydrophilic category, we crafted two samples: the first one was a plasma

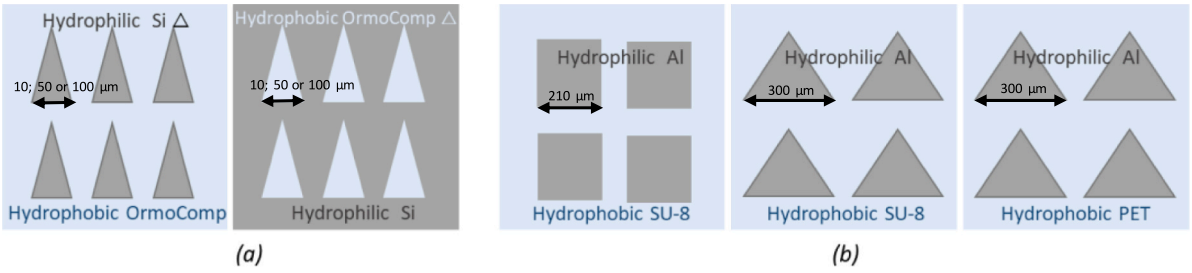

Fig. 1. Prepared patterned samples using: a) UV lithography and plasma treatment, b) metal deposition through a mesh followed by plasma treatment. In the photos, blue color represents hydrophobic zones, and grey color indicates hydrophilic zones. (For interpretation of the references to color in this figure legend, the reader is referred to the web version of this article.)

treated silicon wafer and the second featured an SU-8 film treated with O_2 and CF_4, subsequently coated homogeneously with aluminum. These hydrophilic samples displayed minimal contact angles, measuring less than 10° just after fabrication, and had a surface energy of approximately 40 mN/m. However, due to the surface aging, WCA of both samples increased to reach values greater than 50°.

We prepared also two hydrophobic samples: one underwent plasma treatment on OrmoComp, resulting in a contact angle of 107°, and the other underwent plasma treatment on an SU-8 sample, yielding a contact angle of 135°. Both of these hydrophobic surfaces exhibited a contact angle hysteresis of around 40°. These samples also underwent aging and tended to become less hydrophobic after being in contact with water during water collection tests.

All homogeneous samples are summarized in Table 1. Contact angles were measured every week in order to monitor their properties when used for condensation or collection studies.

These materials were used to fabricate biphilic patterned samples, described in Table 2. The global contact angle of these biphilic surfaces is not accurately indicated, since it can vary due to aging. Regular analyses performed every week show that patterned samples made with OrmoComp polymer are more stable over time, maintaining overall consistent water contact angles. For this reason, these samples were also considered for water condensation tests later. However, samples made with SU-8 polymer tend to become less stable, with water contact angles varying over time. Samples featuring aluminum particles on their surface were the less stable, exhibiting increased hydrophobicity, attributed to the contamination of aluminum particles by carbon present in the surrounding environment [31].

In the case of a variation, the final observed range is indicated in Table 2, and the exact value is mentioned when presenting the water harvesting and condensation results. Bold lines in Table 1 and Table 2 represent the samples that were tested for water collection efficiency.

Samples were characterized by water contact angle measurement using the drop shape analyzer (DSA100) and atomic force microscopy (AFM) (Figure S5).

2.1. Water collection tests

In the water collection tests, we employed a commercial humidifier with a water flow rate of approximately 150 mL/h. This flow was directed into a chamber where the sample was securely positioned on a vertical stand (see Figure S6) with a distance of 25 cm between the humidifier and the surface. Collected water was weighed using a scale. We conducted these tests on reference samples and on patterned samples with triangular patterns, over a duration of two hours, calculating the water collection rates (WCR) in units of milligrams per square centimeter per hour (mg/cm^2/h). These experiments were conducted at room temperature, and the humidity inside the chamber was maintained at levels exceeding 90%. Under these conditions, evaporated water from the water collection jar is estimated to be 20mg g/min. We want to precise that all experiments were conducted in cleanroom, with controlled temperature and humidity ratio; so that the evaporation is stable.

Table 1
Homogeneous samples prepared.

	Samples	Materials	WCA	R_q in nm
Hydrophilic Samples	**Si**	**Hydrophilic Si**	**10° (t_0)- 60° after water collection tests**	**6**
	Al/SU8	Hydrophilic Al	10° (t_0) - 50° after the reaction of Al with the ambient air	164
Hydrophobic Samples	**Ormo**	**Hydrophobic OrmoComp**	**107°**	**15**
	SU8	Hydrophobic SU8	135°	164
	PET	Hydrophobic PET	150°	40

2.2. Water condensation tests

We conducted the tests inside a climatic chamber with a constant temperature of 298K (25°C) and a relative humidity of 90%. To create a temperature contrast, we used a Peltier device (Figure S7) to cool the sample down to 288K. This temperature contrast resulted in a difference of 8 K between the sample's surface temperature and the dew point temperature, which was approximately 296.2 K under the chamber's conditions.

3. Results and discussion

3.1. Water collection efficiency

The results from the water collection tests (Figure 2) confirm findings in the existing literature, highlighting that biphilic samples outperform homogeneous ones [31,32]. Considering the homogeneous surfaces, the water collection rate (WCR) is higher on the hydrophobic surface, as confirmed by Nioras et al [4] who demonstrated that a high droplet mobility is more efficient in the case of fog droplets capture.

Among the biphilic samples depicted in blue in Figure 2, most of the samples exhibit a WCR in the 400-500 mg/cm^2/h range. Nevertheless, these rates are impacted by the evaporation of water from the collection dish, with an evaporation rate of 20 mg/min. If we take into account this evaporation, we can consider that the real water harvesting rate is close to 1.7 g/cm^2/h. This value is comparable to literature where collection rates range between 500 mg/cm^2/h [24,33] and 5 g/cm^2/h [25] depending on fog flow conditions; In the following, we consider the measured values, without taking account the amount of evaporated water for comparison of the different surfaces. The highest WCR of 660 mg/cm^2/h is obtained for sample 13 that corresponds to 300 µm hydrophilic Al triangles surrounded by hydrophobic fluorinated SU8 resist. This distinction could be attributed to various reasons. All the other biphilic surfaces presented in Figure 2 were obtained using OrmoComp polymer, with a lower roughness (Rq = 15 nm) and various triangles with base sizes ranging from 10 µm to 100 µm. But the major difference is that the contact angle of the hydrophobic areas is 135°, that is higher than the hydrophobic fluorinated OrmoComp one which is 107° only. This parameter probably increases the droplet mobility offering a distinct advantage for fog harvesting. This difference is induced by the roughness and the surface chemistry, creating a more pronounced angle contrast within the biphilic sample. These combined characteristics make the sample 13 more effective in water collection.

The PET/Al sample is also characterized by a high angle contrast between the fluorinated PET zones and the Al triangles since homogeneous fluorinated PET exhibits superhydrophobic behavior. However, despite this contrast, the WCR for this sample is low compared to others. The main reason for this behavior is likely due to the superhydrophobic nature of fluorinated PET. Specifically, when the contact angle reaches 150° and the contact angle hysteresis stays below 10°, it leads to extremely mobile droplets that can jump rather than roll. Conversely, on a moderately hydrophobic surface like fluorinated SU8, with a contact angle of 135° and a contact angle hysteresis of 40°, droplets tend to grow into a spherical shape before rolling, aiding in their collection.

Considering the other biphilic surfaces based on hydrophilic silicon and hydrophobic fluorinated resists, we can observe that WCR is not influenced by the patterns' polarity (whether the triangles were made of hydrophobic polymer or hydrophilic silicon), nor by the triangles' dimensions or density. We will see in following results that this behavior is specific to fog harvesting and is different when considering condensation. Additionally, we observe that samples 2 and 3 have an overall hydrophilic surface (with a contact angle of 35°) due to the low density of 10 µm hydrophobic triangles. Despite this, the WCR value in this

Table 2
Prepared samples; △ represents hydrophilic hollow triangles, ▲ represents hydrophobic raised triangles and □ represents hydrophilic aluminum squares.

Samples	Hydrophilic Material	Hydrophobic Material	Patterns shape, base length and tonality	Pitch along X axis	Pitch along Y axis	WCA	R_q in nm
1	Hydrophilic Si (50°)	Hydrophobic OrmoComp (107°)	△ 10 µm	5	5	87°	15
2	**Hydrophilic Si (50°)**	**Hydrophobic OrmoComp (107°)**	**▲ 10 µm**	**10**	**30**	**40°**	**15**
3	**Hydrophilic Si (50°)**	**Hydrophobic OrmoComp (107°)**	**▲ 10 µm**	**20**	**10**	**35°**	**15**
4	**Hydrophilic Si (50°)**	**Hydrophobic OrmoComp (107°)**	**▲ 50 µm**	**50**	**50**	**68°**	**15**
5	**Hydrophilic Si (50°)**	**Hydrophobic OrmoComp (107°)**	**△ 100 µm**	**20**	**20**	**75°**	**15**
6	**Hydrophilic Si (50°)**	**Hydrophobic OrmoComp (107°)**	**▲ 100 µm**	**20**	**20**	**75°-85°**	**15**
7	Hydrophilic Si (50°)	Hydrophobic OrmoComp (107°)	△ 50 µm	50	50	78°-101°	15
8	Hydrophilic Si (50°)	Hydrophobic SU8 (135°)	△ 100 µm	50	20	105°	78
9	Hydrophilic Si (50°)	Hydrophobic SU8 (135°)	△ 100 µm	50	20	115°	164
10	Hydrophilic Si (50°)	Hydrophobic SU8 (135°)	▲ 100 µm	50	20	125°	164
11	Hydrophilic Al (30°)	Hydrophobic SU8 (135°)	□ 210 µm	140	140	56°-77°	78
12	Hydrophilic Al (30°)	Hydrophobic SU8 (135°)	□ 210 µm	140	140	99°	164
13	**Hydrophilic Al (30°)**	**Hydrophobic SU8 (135°)**	**△ 300 µm of Al**	**200**	**200**	**70°-80°**	**78**
Al/PET	**Hydrophilic Al (30°)**	**Hydrophobic PET (150°)**	**△ 300 µm of Al**	**200**	**200**	**135°**	**41**

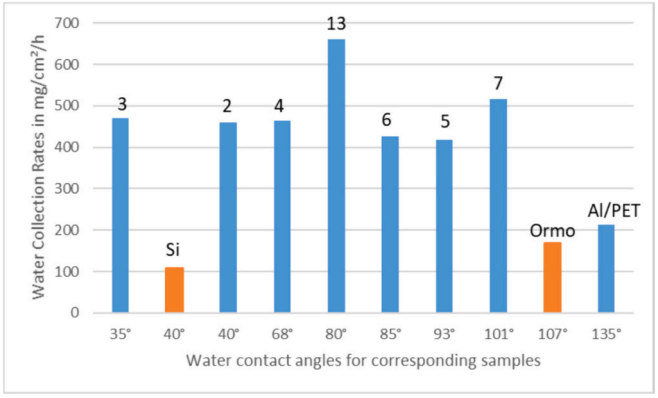

Fig. 2. Water Collection Rate of different samples as a function of the water contact angle. In the photos, blue color represents patterned samples and orange color indicates homogeneous samples. (For interpretation of the references to color in this figure legend, the reader is referred to the web version of this article.)

particular case is comparable to that obtained on other biphilic surfaces with higher contact angles. These results demonstrate that the key parameter is a biphilic surface with moderate hydrophobic areas, and that a higher roughness is advantageous for fog collecting.

However, it is worth noting that during our experiments on a surface with exceptionally high micrometric-level roughness due to the presence of metal aggregates in a polymer matrix, we observed that this excessive roughness hindered droplet sliding, thereby negatively affecting the WCR.

3.2. Theoretical and experimental volume of water droplet departure

To improve the understanding of the obtained results, we calculated the radius (r_{max}) and the volume (V) of the falling drop corresponding to each sample using the equations established by several authors [34,35] in the case of a vertical surface. The falling droplet volume (V) depends on the relation between gravity and adhesion force that is determined by the surface wettability, and therefore the water contact angle θ, the advancing and receding angles θ_a and θ_r, the surface tension σ, and a constant c that represents the deformation of the droplet that equals $\frac{48}{\pi^3} =$ 1.548 [36].

The radius of the falling drop is: $r_{max} = \left(\frac{6c(cos\theta_r - cos\theta_a)sin\theta}{\pi(2-3cos\theta+cos^3\theta)}\frac{\sigma}{\rho g}\right)^{\frac{1}{2}}$ [35] with ρ the water density and g the gravitational acceleration. The falling droplet volume becomes: $V = \pi.r_{max}{}^3\left(\frac{2-3cos\theta+cos^3\theta}{3}\right)$ [36].

We experimentally determined the volume of the sliding droplet using the drop shape analyzer (DSA100), which corresponds to the droplet rolling on the surface when the DSA100 holder is tilted to 90°. Thereafter, we compared these volumes and created the histogram shown in Figure 3.

Our findings can be summarized as follows: Hydrophilic samples with water contact angles less than 60° presented low departure volumes, showing good agreement between theoretical and experimental values, whether the surface is homogeneous or biphilic. These surfaces are so hydrophilic that small droplets fall down easily [37]. Hydrophilic samples with greater contact angles in the range of 60°-80° had higher water departure volumes because droplets grew before rolling off. However, hydrophobic samples with contact angles over 90° had conflicting results. The experimental departure volume exceeded the theoretical value, despite being expected to repel water (hydrophobic). This anomaly was attributed to a high contact angle hysteresis (CAH) of 40°, leading to the loss of superhydrophobicity and subsequent pinning of water droplets to the surface's rough features, causing them to adopt the Wenzel state. This difference was already discussed [38]. It was also concluded in ref [34] that a high CAH is more efficient for water harvesting on surfaces with a high contact angle of 150° to permit the growth of droplets before rolling.

3.3. Water condensation efficiency

Shifting from fog collection to water condensation, we tested six samples to explore various parameters. We monitored the surface changes of these samples under constant conditions: a temperature of 298 K and a relative humidity of 90%, capturing photos every five minutes. Initially we examined homogeneous samples: the hydrophilic sample Al/SU8 with a water contact angle (WCA) of 10° and the hydrophobic SU8 with WCA= 135°. After a 30-minute observation period, it was noteworthy that there were no visible water droplets present on the hydrophilic surface. However, during this time, a thin film had developed on this surface, as depicted in Figure 4. This behavior is typical of hydrophilic surfaces, where nuclei tend to grow and

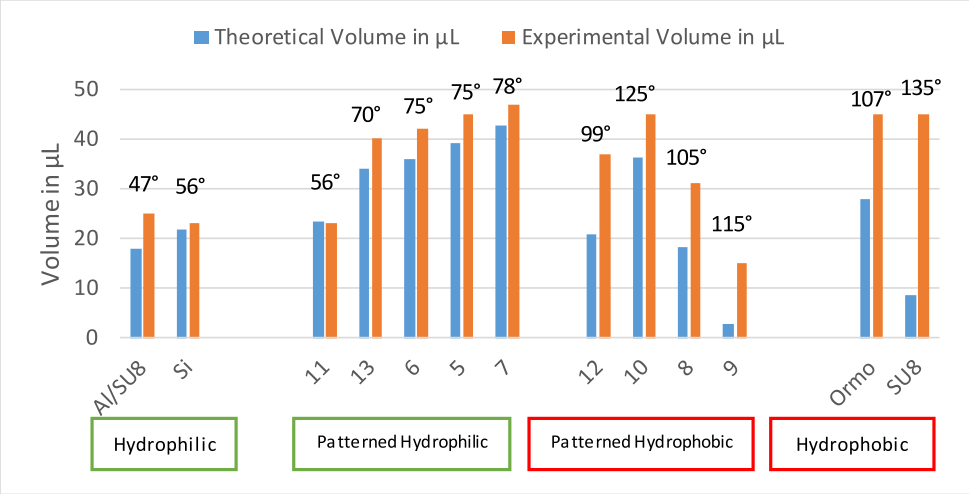

Fig. 3. Theoretical vs experimental volume of droplet departure.

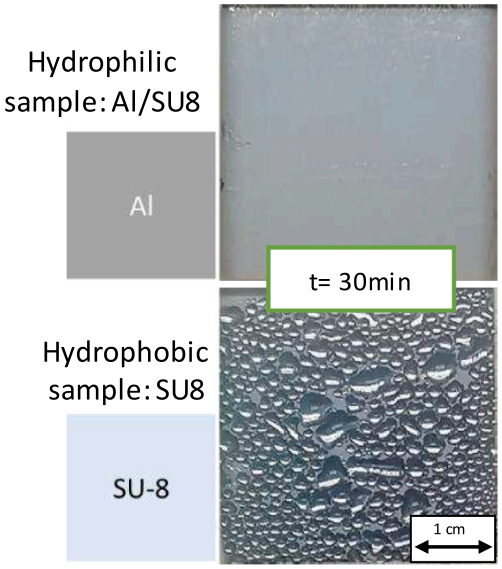

Fig. 4. Condensation photos for homogeneous samples (hydrophilic and hydrophobic) at $t = 30$ min.

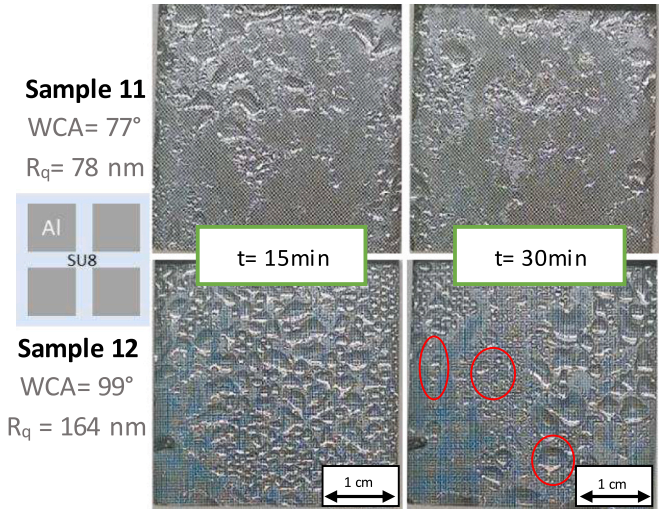

Fig. 5. Condensation photos for samples 11 and 12 at $t = 15$ min and t = 30 min.

eventually cover the surface, resembling the process of filmwise condensation [39]. Conversely, on the hydrophobic surface of SU8, water droplets were observed to increase in size over the 30-minute observation period, yet they did not coalesce. Additionally, no rolling of these droplets was observed, primarily due to the significant contact angle hysteresis (CAH) of 40°, which caused the droplets to strongly adhere to the surface (Figure 4).

In our study of biphilic surfaces, we compared samples that were prepared using the same method: metal deposition through a mask, or lithography in the polymer film. In order to study the role of roughness on water condensation, we used samples created through metal deposition with a mesh: we compared the sample 11, which has low roughness and a WCA of 77°, and sample 12, which has high roughness and a WCA of 99°. At the 15-minute mark, we observed that droplets formed on sample 11 could slide off rapidly, (Figure 5), whereas on sample 12, they took more time to coalesce and increase in size before rolling off (Figure 5). By the 30-minute mark, some droplets on sample 11 had slid down, but no new droplets had formed. On the rougher sample, new water droplets appeared at 30 minutes in these areas after first droplet rolling. The reason for this difference is that in sample 11, when droplets fall from the surface, they create a film that prevents new drops from forming. On the other hand, in sample 12, the rough surface and the higher contact angle favor dropwise condensation and drops regeneration. The higher roughness is therefore advantageous for dew condensation.

Next, we compared samples prepared using lithography to evaluate the impact of pattern size and density on dew condensation: we selected sample 6, featuring hydrophobic triangles with a base length of 100 µm in a hydrophilic background resulting in a WCA of 77°, and sample 1 which has hydrophilic triangles with a base length of 10 µm in a hydrophobic background. On sample 6, drops started sliding at 20 minutes (Figure 6), whereas on sample 1, no drops had slid by that time.

At the 25-minute mark, new drops appeared in areas free of rolling drops, on the surface of sample 6, while the first drop slid from the surface of sample 1 but without further new droplets nucleation. This behavior was confirmed after longer time. The interpretation of the results is influenced by sample 1's design in two key ways. First, its limited hydrophilic zones, due to small and sparse triangles, results in few nucleation sites, making the nucleation process highly random. Second, the triangles are 10 times larger on sample 6 (100 µm compared to 10 µm) and the triangles are hydrophobic, surrounded by hydrophilic Si. This design favors dropwise condensation with circular droplets. Other

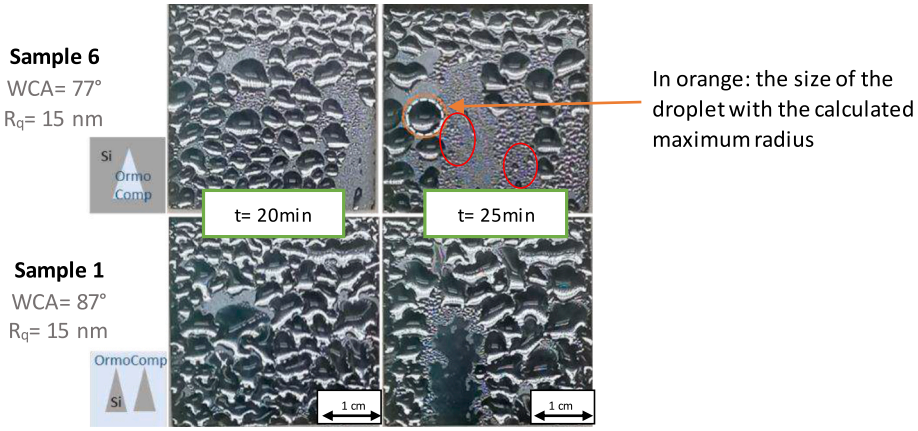

Fig. 6. Condensation photos for samples 6 and 1 at $t = 20$ min and $t = 25$ min.

experiments performed on similar surfaces with square patterns with dimensions ranging from 10μm to 500μm also demonstrated that 100 μm hydrophobic structures are promoting dew condensation thanks to circular droplets easily rolling after coalescence and growth. This suggests that unlike fog collection, the size of the pattern does impact the dew collection rate. However, the discrepancy in water harvesting rates in this scenario is not particularly significant. Through our condensation experiments, we determined that the order of dew water collection rate (WCR) is 90 mg/cm^2/h, which is approximately five times lower than the fog WCR on similar surfaces. This distinction between fog and dew WCR has been previously noted in reference [4]. The 90 mg/cm^2/h condensation rate was obtained in the following conditions: 80% humidity ratio, 30°C in the climatic chamber, $\Delta T = 12$k between the cooled surface and the dew point, and $\Delta\omega = 21$ $g_{water}/kg_{dry\ air}$. This rate is comparable to the one obtained in ref [40] on hierarchical Al and Cu rough surfaces, and on the biphilic surface prepared in reference [12].

In Sample 6, we observed large circular droplets. Using pictures, we measured the radius of a specific droplet marked in white, finding it to be 2.9 mm. Considering the equation established in reference [35] and mentioned above, the calculated radius of a falling droplet was 3.5 mm. To assess the variance between both radii, we illustrated on Figure 66 the experimental droplet size in white and the calculated theoretical size in orange. The theoretical droplet size appears to be slightly bigger. This comparison is coherent since the same order of magnitude is obtained, taking into account the low accuracy of the experimental measurement and the fact that it is determined before drop rolling.

The present goal is to refine design rules impacting water harvesting. These model surfaces will help in optimizing surfaces with more durable and cost-effective materials and processes.

4. Conclusion

This work presented a comprehensive analysis of sample capabilities in collecting water from fog featuring small water droplets and condensing water from dew. The present goal was to refine design rules impacting water harvesting. For this purpose, three types of patterned samples were fabricated using and combining lithography, metal deposition and plasma roughening while carefully exploring diverse patterns, sizes, roughness levels, wettability characteristics, and chemical compositions. The findings demonstrate the superiority of biphilic patterned samples in both water collection and condensation processes. However, our study also showed that samples ideal for efficient water collection may not necessarily be optimal for water condensation, highlighting the nuanced nature of these mechanisms. Our research helps the design of surfaces for water harvesting, which can be valuable for improving water collection methods in the future. These model surfaces will help in optimizing surfaces with more durable and cost-effective materials and processes.

Declaration of competing interest

The authors declare that they have no known competing financial interests or personal relationships that could have appeared to influence the work reported in this paper.

Data availability

No data was used for the research described in the article.

Acknowledgements

The authors would like to thank the French national nanofabrication network (RENATECH) for its support.

Appendix A. Supplementary data

Supplementary data to this article can be found online at https://doi.org/10.1016/j.mne.2024.100255.

References

[1] UNICEF, Water Scarcity: Addressing the Growing Lack of Available Water to Meet Children's Needs [Online]. Available, https://www.unicef.org/wash/water-scarcity, 2024.
[2] B. Bhushan, Design of water harvesting towers and projections for water collection from fog and condensation, Philos. Trans. R. Soc. A Math. Phys. Eng. Sci. 378 (2167) (Mar. 2020) 20190440, https://doi.org/10.1098/rsta.2019.0440.
[3] H. Sun, et al., Bioinspired micro- and nanostructures used for fog harvesting, Appl. Phys. A Mater. Sci. Process. 127 (6) (Jun. 2021) 461, https://doi.org/10.1007/s00339-021-04619-1.
[4] D. Nioras, K. Ellinas, V. Constantoudis, E. Gogolides, How different are fog collection and dew water harvesting on surfaces with different wetting behaviors? ACS Appl. Mater. Interfaces 13 (40) (Oct. 2021) 48322–48332, https://doi.org/10.1021/acsami.1c16609.
[5] Z. Ahrestani, S. Sadeghzadeh, H.B. Motejadded Emrooz, An overview of atmospheric water harvesting methods, the inevitable path of the future in water supply, RSC Adv. 13 (15) (2023) 10273–10307, https://doi.org/10.1039/D2RA07733G.
[6] M.S. Thavalengal, et al., Progress and prospects of air water harvesting system for remote areas: a comprehensive review, Energies 16 (6) (Mar. 2023) 2686, https://doi.org/10.3390/en16062686.
[7] X. Wang, J. Zeng, J. Li, X. Yu, Z. Wang, Y. Zhang, Beetle and cactus-inspired surface endows continuous and directional droplet jumping for efficient water harvesting, J. Mater. Chem. A 9 (3) (2021) 1507–1516, https://doi.org/10.1039/D0TA10123K.
[8] P. Zhu, R. Chen, C. Zhou, Y. Tian, L. Wang, Asymmetric fibers for efficient fog harvesting, Chem. Eng. J. 415 (Jul. 2021) 128944, https://doi.org/10.1016/j.cej.2021.128944.
[9] Z. Chen, Z. Zhang, Recent progress in beetle-inspired superhydrophilic-superhydrophobic micropatterned water-collection materials, Water Sci. Technol. (Jun. 2020) wst2020238, https://doi.org/10.2166/wst.2020.238.

[10] D. Nioras, K. Ellinas, E. Gogolides, Atmospheric water harvesting on Micro-nanotextured Biphilic surfaces, ACS Appl. Nano Mater. 5 (8) (Aug. 2022) 11334–11341, https://doi.org/10.1021/acsanm.2c02439.
[11] Y. Jiang, C. Machado, K.K. Park, From capture to transport: a review of engineered surfaces for fog collection, Droplet 2 (2) (Apr. 2023) e55, https://doi.org/10.1002/dro2.55.
[12] Y. Hou, Y. Shang, M. Yu, C. Feng, H. Yu, S. Yao, Tunable water harvesting surfaces consisting of Biphilic nanoscale topography, ACS Nano 12 (11) (Nov. 2018) 11022–11030, https://doi.org/10.1021/acsnano.8b05163.
[13] W. Zhou, et al., Efficient fabrication of desert beetle-inspired micro/nano-structures on polypropylene/graphene surface with hybrid wettability, chemical tolerance, and passive anti-icing for quantitative fog harvesting, Chem. Eng. J. 453 (Feb. 2023) 139784, https://doi.org/10.1016/j.cej.2022.139784.
[14] N. Bakhtiari, S. Azizian, B. Jaleh, Hybrid superhydrophobic/hydrophilic patterns deposited on glass by laser-induced forward transfer method for efficient water harvesting, J. Colloid Interface Sci. 625 (Nov. 2022) 383–396, https://doi.org/10.1016/j.jcis.2022.06.039.
[15] H. Zhang, Y. Liu, Z. Zhang, M. Hua, G. Dong, A superhydrophobic surface patterned with hydrophilic channels for directional sliding control and manipulation of droplets, Surf. Coat. Technol. 409 (Mar. 2021) 126836, https://doi.org/10.1016/j.surfcoat.2021.126836.
[16] S. Lee, J. Lee, Improvement of humid air condensate drainage through bi-philic patterned surfaces, Int. J. Heat Mass Transf. 194 (Sep. 2022) 123097, https://doi.org/10.1016/j.ijheatmasstransfer.2022.123097.
[17] P.S. Mahapatra, A. Ghosh, R. Ganguly, C.M. Megaridis, Key design and operating parameters for enhancing dropwise condensation through wettability patterning, Int. J. Heat Mass Transf. 92 (Jan. 2016) 877–883, https://doi.org/10.1016/j.ijheatmasstransfer.2015.08.106.
[18] D. Feldmann, B.-E. Pinchasik, The temperature dependent dynamics and periodicity of dropwise condensation on surfaces with wetting heterogeneities, J. Colloid Interface Sci. 644 (Aug. 2023) 146–156, https://doi.org/10.1016/j.jcis.2023.04.060.
[19] D. Gurera, B. Bhushan, Designing bioinspired surfaces for water collection from fog, Philos. Trans. R. Soc. A Math. Phys. Eng. Sci. 377 (2138) (Feb. 2019) 20180269, https://doi.org/10.1098/rsta.2018.0269.
[20] Y. Guo, et al., Patterned hybrid wettability surfaces for fog harvesting, Langmuir 39 (13) (Apr. 2023) 4642–4650, https://doi.org/10.1021/acs.langmuir.2c03432.
[21] D. Xing, R. Wang, F. Wu, X. Gao, Confined growth and controlled coalescence/self-removal of condensate microdrops on a spatially heterogeneously patterned superhydrophilic–superhydrophobic surface, ACS Appl. Mater. Interfaces (Jun. 2020), https://doi.org/10.1021/acsami.0c04922 acsami.0c04922.
[22] J. Feng, L. Zhong, Z. Guo, Sprayed hieratical biomimetic superhydrophilic-superhydrophobic surface for efficient fog harvesting, Chem. Eng. J. 388 (May 2020) 124283, https://doi.org/10.1016/j.cej.2020.124283.
[23] W. Huang, et al., Cellulose-based superhydrophobic surface decorated with functional groups showing distinct wetting abilities to manipulate water harvesting, ACS Appl. Mater. Interfaces 12 (36) (Sep. 2020) 40968–40978, https://doi.org/10.1021/acsami.0c12504.
[24] X. Gou, Z. Guo, Hybrid Hydrophilic–Hydrophobic CuO@TiO $_2$ -coated copper mesh for efficient water harvesting, Langmuir 36 (1) (Jan. 2020) 64–73, https://doi.org/10.1021/acs.langmuir.9b03224.
[25] Y. Zhang, T. Wang, M. Wu, W. Wei, Durable superhydrophobic surface with hierarchical microstructures for efficient water collection, Surf. Coat. Technol. 419 (Aug. 2021) 127279, https://doi.org/10.1016/j.surfcoat.2021.127279.
[26] F. Zhang, Z. Guo, Bioinspired materials for water-harvesting: focusing on microstructure designs and the improvement of sustainability, Mater. Adv. 1 (8) (2020) 2592–2613, https://doi.org/10.1039/D0MA00599A.
[27] C.-W. Lo, Y.-C. Chu, M.-H. Yen, M.-C. Lu, Enhancing condensation heat transfer on three-dimensional hybrid surfaces, Joule 3 (11) (Nov. 2019) 2806–2823, https://doi.org/10.1016/j.joule.2019.08.005.
[28] X. Ji, D. Zhou, C. Dai, J. Xu, Dropwise condensation heat transfer on superhydrophilic-hydrophobic network hybrid surface, Int. J. Heat Mass Transf. 132 (Apr. 2019) 52–67, https://doi.org/10.1016/j.ijheatmasstransfer.2018.11.139.
[29] D. Boylan, D. Monga, L. Shan, Z. Guo, X. Dai, Pushing the limit of beetle-inspired condensation on Biphilic quasi-liquid surfaces, Adv. Funct. Mater. 33 (11) (Mar. 2023) 2211113, https://doi.org/10.1002/adfm.202211113.
[30] T.-Y. Zhang, L.-W. Mou, J.-Y. Zhang, L.-W. Fan, J.-Q. Li, A visualized study of enhanced steam condensation heat transfer on a honeycomb-like microporous superhydrophobic surface in the presence of a non-condensable gas, Int. J. Heat Mass Transf. 150 (Apr. 2020) 119352, https://doi.org/10.1016/j.ijheatmasstransfer.2020.119352.
[31] V.J. Rico, et al., Hydrophobicity, freezing delay, and morphology of laser-treated aluminum surfaces, Langmuir 35 (19) (May 2019) 6483–6491, https://doi.org/10.1021/acs.langmuir.9b00457.
[32] V. Sharma, K. Yiannacou, M. Karjalainen, K. Lahtonen, M. Valden, V. Sariola, Large-scale efficient water harvesting using bioinspired micro-patterned copper oxide nanoneedle surfaces and guided droplet transport, Nanoscale Adv. 1 (10) (2019) 4025–4040, https://doi.org/10.1039/C9NA00405J.
[33] S.J. Lee, N. Ha, H. Kim, Superhydrophilic–Superhydrophobic water harvester inspired by wetting property of Cactus stem, ACS Sustain. Chem. Eng. 7 (12) (Jun. 2019) 10561–10569, https://doi.org/10.1021/acssuschemeng.9b01113.
[34] J. Lu, et al., Bioinspired hierarchical surfaces fabricated by femtosecond laser and hydrothermal method for water harvesting, Langmuir 35 (9) (Mar. 2019) 3562–3567, https://doi.org/10.1021/acs.langmuir.8b04295.
[35] S. Kim, K.J. Kim, Dropwise condensation modeling suitable for superhydrophobic surfaces, J. Heat Transf. 133 (8) (Aug. 2011) 081502, https://doi.org/10.1115/1.4003742.
[36] D. Beysens, The Physics of Dew, Breath Figures and Dropwise Condensation, vol. 994. in Lecture Notes in Physics, vol. 994, Springer International Publishing, Cham, 2022, https://doi.org/10.1007/978-3-030-90442-5.
[37] A.I. ElSherbini, A.M. Jacobi, Retention forces and contact angles for critical liquid drops on non-horizontal surfaces, J. Colloid Interface Sci. 299 (2) (Jul. 2006) 841–849, https://doi.org/10.1016/j.jcis.2006.02.018.
[38] Y. Wang, et al., Sustainable Superhydrophobic surface with tunable nanoscale hydrophilicity for water harvesting applications, Angew. Chem. Int. Ed. 61 (10) (Mar. 2022), https://doi.org/10.1002/anie.202115238.
[39] Y. Hou, M. Yu, X. Chen, Z. Wang, S. Yao, Recurrent filmwise and dropwise condensation on a beetle mimetic surface, ACS Nano 9 (1) (Jan. 2015) 71–81, https://doi.org/10.1021/nn505716b.
[40] T.M. Thomas, P. Sinha Mahapatra, R. Ganguly, M.K. Tiwari, Preferred mode of atmospheric water vapor condensation on nanoengineered surfaces: dropwise or filmwise? Langmuir 39 (15) (Apr. 2023) 5396–5407, https://doi.org/10.1021/acs.langmuir.3c00022.